Direct Optical Lithography of $CsPbX_3$ Nanocrystals via Photoinduced Ligand Cleavage with Post-Patterning Chemical Modification and Electronic Coupling

Jia-Ahn Pan[†], Justin C. Ondry[†], Dmitri V. Talapin[*,†,‡]

† *Department of Chemistry, James Franck Institute, and Pritzker School of Molecular Engineering, University of Chicago, Chicago, Illinois 60637, United States*

‡ *Center for Nanoscale Materials, Argonne National Laboratory, Argonne, Illinois 60439, United States*

Keywords: Direct optical lithography, perovskite nanocrystal, photosensitive ligand, anion exchange, ligand exchange

TOC graphic

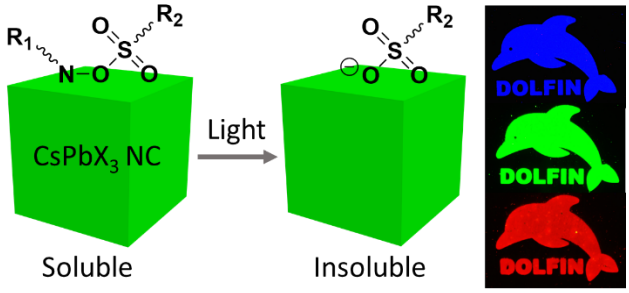

Abstract

Microscale patterning of solution-processed nanomaterials is important for integration in functional devices. Colloidal lead halide perovskite (LHP) nanocrystals (NCs) can be particularly challenging to pattern due to their incompatibility with polar solvents and lability of surface ligands. Here, we introduce a direct photo-patterning approach for LHP NCs through the binding and subsequent cleavage of a photosensitive oxime sulfonate ester (–C=N–OSOO–). The photosensitizer binds to the NCs through its sulfonate group and is cleaved at the N–O bond during photo-irradiation with 405 nm light. This bond cleavage decreases the solubility of the NCs which allows patterns to emerge upon development with toluene. Post-patterning ligand exchange results in photoluminescence quantum yields up to 76%, while anion exchange provides tunability in the emission wavelength. The patterned NC films show photoconductive behavior, demonstrating that good electrical contact between the NCs can be established.

Main Text

Colloidal lead halide perovskite (LHP) nanocrystals (NCs) have been intensely investigated due to their facile solution-phase syntheses, defect tolerance, and fascinating optoelectronic properties.[1-4] LHP NCs have been researched for use in light emitting diodes (LEDs),[5-7] color conversion filters,[8] lasers,[9-11] solar cells,[12-13] visible-light photodetectors,[14] X-ray scintillators,[15-16] and quantum emitters.[17] As the library of LHP NCs and perovskite-related nanomaterials continue to expand toward increased complexity, there is a need to develop methods for integrating LHP NCs in practical devices. In particular, the NCs need to be controllably deposited as a two-dimensional pattern for proper interfacing with other electronic and photonic components. This patterning process is also required for the integration of LHP NCs in many display technologies.

Various approaches to patterning perovskite nanomaterials have been reported including micro/nano-imprinting,[18-19] ink jet printing,[20-21] X-ray lithography,[22] electron-beam lithography,[23] and photolithography. Among these techniques, photolithography is a particularly attractive route due to its high resolution, high throughput, and wide availability. Unfortunately, the ionic nature of LHP NCs typically makes them incompatible with traditional photolithography workflows that use polar solvents. To overcome this issue, modifications to either the NCs or the photolithography

process have been explored such as using silica-encapsulated LHP NCs,[8] orthogonal fluorinated photoresist and developer,[24] and adding a self-healing recrystallization step.[9]

Alternatively, LHP NCs can be photopatterned directly by including a photosensitive component into the LHP NC solution (or LHP NC precursor solution). This can be done by using cross-linkable ligands,[25-28] embedding the LHP NCs in a monomer matrix that can be photo-polymerized,[29] or *in situ* crystallization of LHP NCs in an oxide/polymer matrix with a pulsed laser.[30-31] These approaches typically result in a patterned nanocomposite consisting of LHP NCs dispersed in an insulating matrix, which can be helpful for increasing the chemical stability of the LHP NCs. However, this process prevents electrical contact with the NCs, which is crucial for devices such as LEDs and photodetectors. Furthermore, the NCs in these nanocomposites are sealed off from further chemical manipulations such as ligand and ion exchanges. Also, the large separation between LHP NCs in a matrix would preclude any coherent coupling effects such as superfluorescence.[32-33]

We recently introduced a patterning approach for colloidal nanomaterials which we call direct optical lithography of functional inorganic nanomaterials (DOLFIN).[34-35] The DOLFIN approach involves the use of small-molecule photosensitizers that interact with the NC surface upon light exposure, allowing the solubility of the NCs to be modulated, forming micropatterns. We have used this framework to develop a library of photosensitive ligand chemistry for patterning semiconductor, dielectric, metallic and magnetic NCs. In parallel, we have demonstrated the fabrication of various high-performing patterned devices such as transistors, LEDs, and diffractive optical elements.[35-37] However, these methods typically involve polar solvents such as DMF and/or ligand-exchange reactions, both of which degrade LHP NCs.

Here, we explore the direct optical lithography of $CsPbBr_3$ and $CsPbBr_{3-x}Cl_x$ LHP NCs through a light-induced ligand cleavage mechanism. A photosensitive oxime sulfonate ester (–C=N–OSOO–) is first mixed with the NCs to displace some of the native ligands. Upon irradiation of 405 nm light through a mask, the photosensitive ligand cleaves, rendering the NCs insoluble in toluene and resulting in micro-scale patterns. Post-patterning ligand exchange replaces the sulfonate ligand with more appropriate ligands that can better passivate the NC surfaces, increasing the absolute photoluminescence quantum yield (PLQY) of patterned films up to 76%. Furthermore, post-patterning anion exchange allows the emission wavelength to be tuned across

the visible spectrum. Finally, we demonstrate that the patterned NC layer behaves as a photoconductor when illuminated with visible light. Together our results demonstrate a versatile process for patterning LHP NCs which are chemically and electronically accessible.

$CsPbBr_3$ NCs capped with oleic acid (OAc) and oleylamine (OAm) were prepared using a modified benzoyl halide hot injection method.[38] These NCs were then mixed with a solution of a photosensitive oxime sulfonate ester such as PA-480, which partially replaced the native ligands (Scheme 1). This solution was then spin-coated to form a film, which was then irradiated with 405 nm light through a mask. This light exposure decomposes the photosensitive PA-480, reducing the solubility of the NCs in the toluene developer and results in a patterned film. Finally, the patterned films can be treated with a variety of solutions that allow for ligand and/or anion exchange.

Scheme 1. Outline of the processing steps for direct photolithography of $CsPbX_3$ LHP NCs with the photosensitive oxime sulfonate ester.

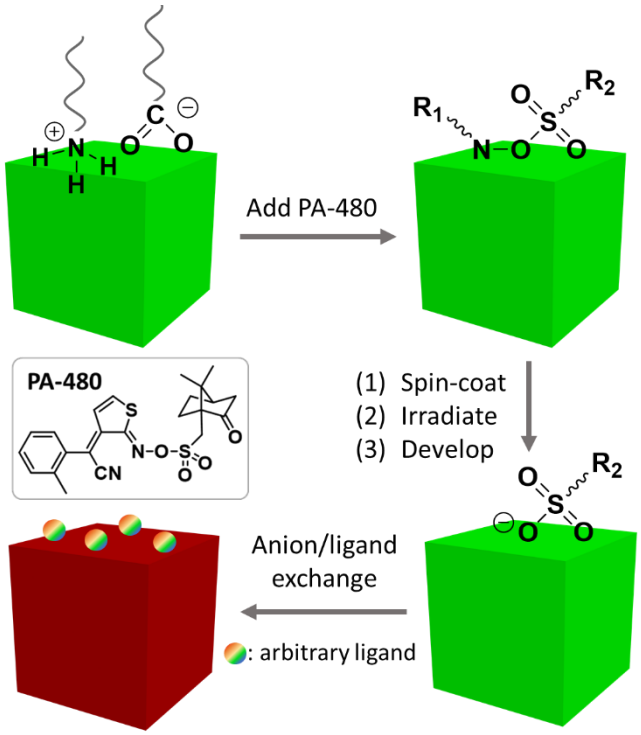

The patterned $CsPbBr_3$ NC films were visibly luminescent as viewed under a fluorescence optical microscope with features sizes as small as 1 μm (Figure 1A–C). However, the PLQY immediately after development with toluene was low (< 5%), which we attribute to the poor ability of the sulfonate ligand to passivate surface defects, combined with partial removal of labile surface

ligands by excess toluene. Hence, we investigated the use of several solution-phase treatments to further improve the PLQY. Many chemical treatments to improve the PLQY of LHP NCs have been reported,[39-44] but we had to adapt these methods as a film-based treatment. We found that film-treatments had to be carried out in a non-solvent such as ethyl acetate to prevent redissolution of the patterned films. After screening several combinations of ligands and other additives, we found that two successive spin-coating treatments with an ethyl acetate solution of $PbBr_2$, octanoic acid (OctAc) and butylamine (BuAm) increased the film PLQY to 79% (Figure 1E). The PL lifetime after this $PbBr_2$/OctAc/BuAm treatment was also longer (τ_{avg} = 7.3 ns) compared to the as-synthesized $CsPbBr_3$ OAm/OAc NCs (τ_{avg} = 4.8 ns), as shown in Figure S10. OcAc and BuAm react to form butylammonium octanoate, which binds to the NC surface as X-type ligands similar to oleylammonium oleate.[45] However, butylammonium octanoate is significantly smaller than oleylammonium oleate which should allow it to better penetrate through the nano-porous film. At the same time, $PbBr_2$ has been reported to introduce excess Br^- anions which also help passivate the NC surface.[40] We also investigated the effect of adding trifluoroacetate (TFA) ions, which has been found to bind stronger to the surface lead ions, leading to better passivation.[39] TFA is also smaller than OctAc and should increase the electronic contact between the NCs. When a treatment of $PbBr_2$/OctAc/BuAm/TFA was used, the PLQY was roughly the same (76%), but the PL lifetime was slightly reduced (τ_{avg} = 3.5 ns), which is consistent with an increase in electronic coupling. Finally, we note that the PLQY values attained through this film treatment method is still lower than the reported >95% obtained by solution-phase treatment,[40] which could be due to inaccessibility of a small amount of unpassivated surface sites after film deposition.

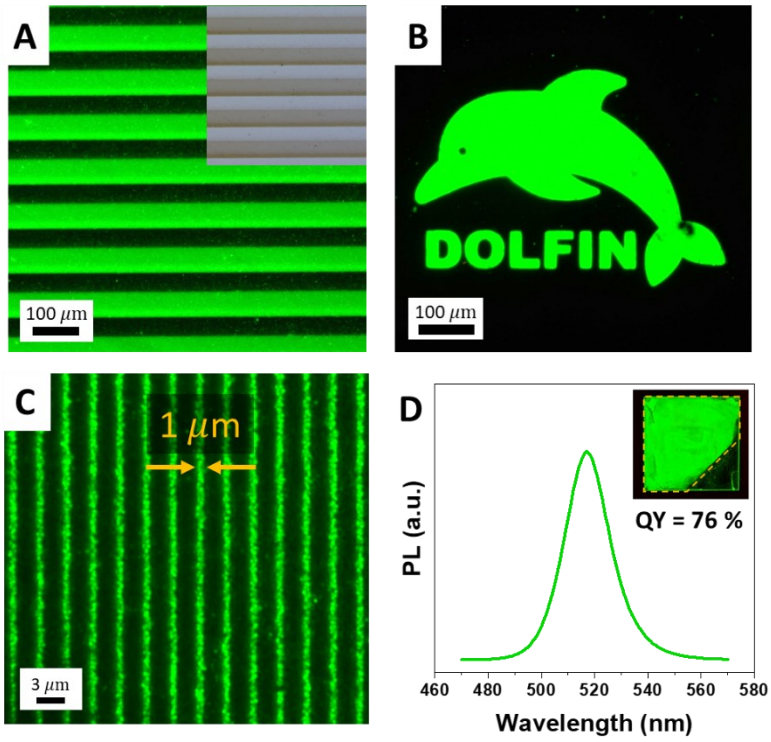

E

Treatment on patterned film	PLQY $\pm \sigma$ (%)
No treatment	< 5
Trifluoroacetic acid + butylamine	37 ± 3
$PbBr_2$ + octanoic acid + butylamine	79 ± 2
$PbBr_2$ + octanoic acid + butylamine + trifluoroacetic acid	76 ± 3

Figure 1. (A-C) Fluorescence optical microscope images of micro-patterned films of $CsPbBr_3$ NCs with the PA-480 photosensitizer. Inset in (A): Bright-field optical microscope image. (D) Photoluminescence (PL) spectrum of a $CsPbBr_3$ film (PLQY = 76%) after patterning with PA-480 followed by treatment with a mixture of $PbBr_2$, octanoic acid, butylamine and trifluoroacetic acid in ethyl acetate. Inset: Photograph of the film under ultraviolet light. The dotted orange line indicates the region exposed to 405 nm light during the patterning process. (E) Table showing the PLQY of patterned $CsPbBr_3$ films with various of post-patterning treatments.

To elucidate the patterning mechanism, we investigated the changes that occur during each step of the patterning process (Figure 2). First, we measured the absorption and PL spectra of solutions and films containing LHP NCs and PA-480 (Figure 2A and S1) and found that the absorption onset of the LHP NCs (~510 nm) does not change appreciably at each step of the process. Also, the shape of the PL peak at 512 nm does not change upon the addition of PA-480

and red-shifts by only 1 nm (to 513 nm) after irradiation in solution. The solution PLQY drops from 31% to 19% after addition of PA-480 but recovers to 23% after irradiation (Figure S9). For films, the PL spectra further red-shifts by about 5 nm (to about 517 nm) after patterning and treatment (Figure 1D), which is consistent with coupling between the NCs. On the other hand, the absorption peak of PA-480 at ~400 nm (superimposed on the absorption spectrum of LHP NCs) clearly changes upon photoirradiation with 405 nm light. Since similar absorption changes were observed when PA-480 was irradiated in the absence of LHP NCs (Figure S2), we infer that the photodecomposition process of PA-480 (Figure S3) is not significantly affected by the presence of the LHP NCs.

Next, to better understand the photopatterning chemistry, we carried out film FTIR spectroscopy to probe changes in the ligand shell of the LHP NCs (Figure 2B and S6). Conveniently, PA-480 has several distinct IR absorption peaks: C≡N (2201 cm^{-1}), C=O (1746 cm^{-1}), S=O (1068 cm^{-1}, 1054 cm^{-1}) and N–O (894 cm^{-1}, 852 cm^{-1}, 798 cm^{-1}). The N–O peaks were assigned based on previous reports and on the observation that these peaks completely disappear upon photoirradiation (Figure S6).[46-47] The as-synthesized $CsPbBr_3$ NCs have mostly broad absorption peaks in the 1750–940 cm^{-1} region, which can be assigned to bound oleylammonium and oleate ligands. Upon addition of PA-480 to the NCs, the resulting FTIR spectrum looks similar to a superposition of the PA-480 and the NC spectra aside from two important changes: (1) the appearance of a peak at 1708 cm^{-1} which can be distinctively assigned to free oleic acid (indicating that it has been displaced),[1, 48] and (2) the red-shift of the S=O peaks to 1035 cm^{-1}, which has been previously assigned to a surface-bound sulfonate group.[49] To preserve charge neutrality, we believe that oleylammonium ligands are also displaced together with the oleate, although the bound or unbound state of oleylammonium is harder to verify by FTIR due to interfering peaks. In other words, we hypothesize that the X-type oleylmmonium oleate ion pair has been replaced by the neutral L-type PA-480 ligand, which binds through the sulfonate oxygen atoms. Upon irradiation, the N–O peaks vanish, indicating the complete cleavage of PA-480. After development with toluene, the C=O and S=O peaks remain strongly present, which means that the sulfonate fragment (that contains the ketone group) stays attached to the NC surface. In contrast, the C≡N peaks are no longer present, which implies that the cyanide fragment has been washed away during this step. Finally, treatment of the film with trifluoroacetic acid/butylamine dissolved in ethyl acetate reveals that all the peaks of the sulfonate ligand (C=O and S=O) are replaced by bound trifluoroacetate

peaks (COO^-: 1676 cm^{-1}, C–F: 1220–1110 cm^{-1}). Hence, although the sulfonate group resists dissolution in the toluene developer, it can still be substituted by other surface ligands that have an even stronger affinity for the NC surface. This allows for further tunability of the ligand shell, which is important to achieve good material performance.

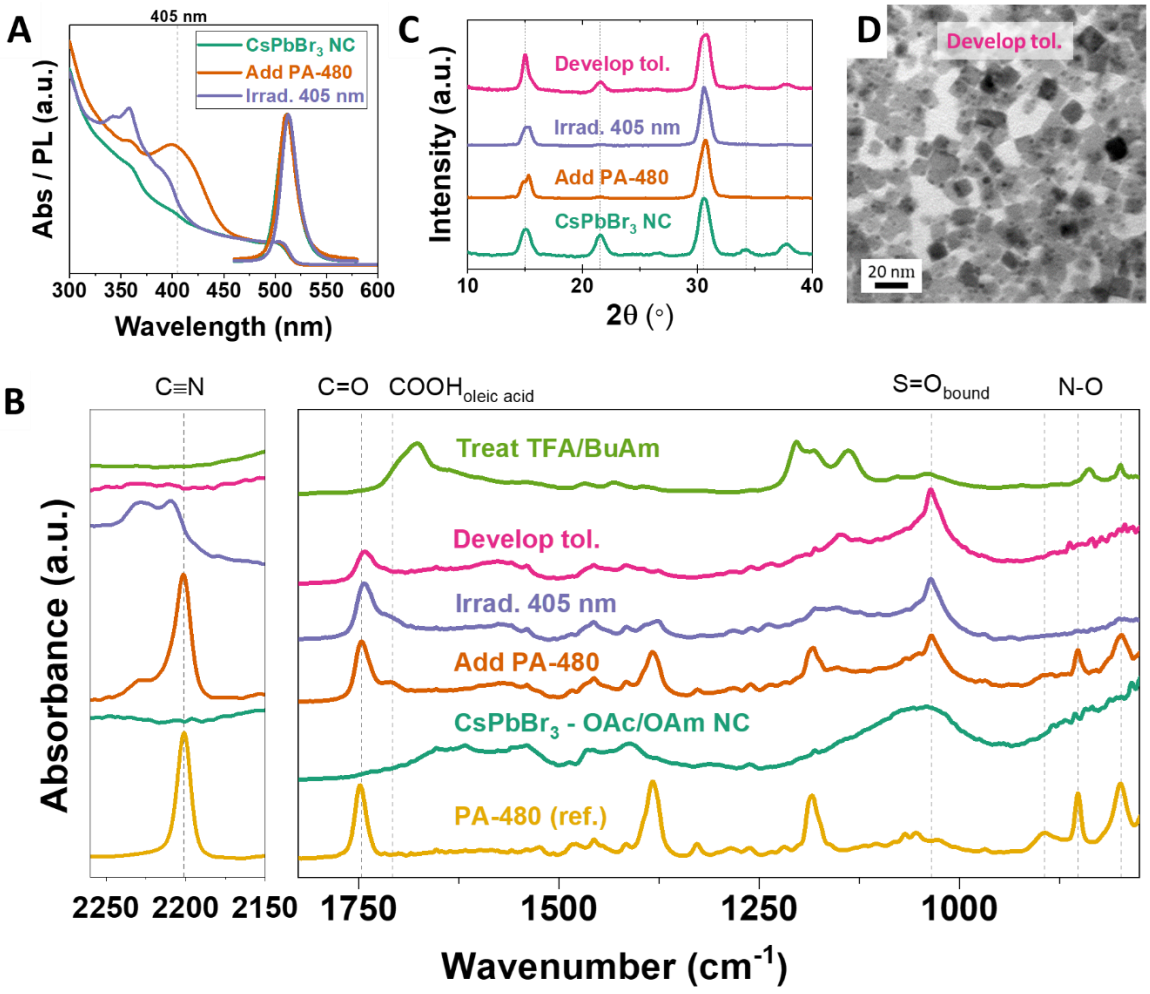

Figure 2. Investigation of the $CsPbBr_3$ NCs and their ligands after each step of the DOLFIN patterning process. (A) Solution-phase absorption and photoluminescence spectra of $CsPbBr_3$ NCs as synthesized, after the addition of PA-480, and after irradiation with 405 nm light. (B) FTIR absorption spectra of $CsPbBr_3$ NCs as synthesized, after the addition of PA-480, irradiation with 405 nm light, development with toluene, and post-patterning treatment with a trifluoroacetic acid/butylamine (TFA/BuAm) mixture in ethyl acetate. The spectra of a PA-480 film is also plotted for reference. (C) Powder X-ray diffraction (XRD) spectra as synthesized, after the addition of PA-480, irradiation with 405 nm light and development with toluene. (D) Transmission electron microscope (TEM) images of the $CsPbBr_3$ NCs after development.

Additionally, we used powder X-ray diffraction (XRD) and transmission electron microscopy (TEM) to explore how our patterning chemistry affects the inorganic LHP nanostructure. XRD analysis shows that the orthorhombic $CsPbBr_3$ diffraction peaks are retained throughout the patterning process with no new crystalline phases (Figure 2C). Careful examination of the pseudo-cubic (100) peaks ($2\theta \sim 15°$) reveal subtle differences in the peak splitting profile at each step. One possibility is the splitting of the (100) peak can be attributed to interference effects from superlattice formation. This has been recently explained using a multilayer diffraction model.[50] We obtained a reasonable fit the (100) and the (200) peaks ($2\theta \sim 30.5°$), which shows that the differences in the peak profile can be accounted for by variations in the NC ordering (Figure S4). Based on this, the differences observed in the XRD patterns during the patterning treatments likely are not a result of changes to the inorganic core of the nanocrystal. This is further supported by a UV-vis absorption of the developed films which do not contain sharp features in the 300–350 nm range, which is where several LHP decomposition products can appear (Figure S1).[51-52] Transmission electron microscopy (TEM) reveals that the average size of the LHP NCs remains constant at about 10 ± 2 nm throughout the entire patterning process (Figure S5). The NCs were found to be well separated after the addition of PA-480 and irradiation but had significant necking upon development with toluene (Figure 2D).

To summarize our mechanistic studies, we obtained results consistent with a patterning mechanism involving the photoinduced cleavage of a bound oxime sulfonate ligand. The binding of the sulfonate ligand is supported both by the detection of free oleic acid and bound sulfonate signals. Photoirradiation and development result in the cleavage of the ligand, leaving behind a bound sulfonate group that reduces the LHP NC solubility in toluene. This solubility change is likely due to the increase in the polarity of the ligands after decomposition: a relatively large, non-polar, aryl ligand is cleaved into a shorter, polar ketone ligand. In addition, this mechanism is also supported by the successful patterning of LHP NCs using an imido sulfonate ester (ILP-110N) which has the same cleavable –N–OSOO– motif but with different side groups (Figure S7). The patterns formed with ILP-110N also had good contrast but was more prone to cracking, which we attribute to limited substrate adhesion of the perflorinated butyl chain.

The emission wavelength of the LHP NC patterns can also be tuned across the visible spectrum by modifying its halide composition (Figure 3).[53-54] This can be done by synthesizing

LHP NCs with different halide compositions, or through a post-patterning anion-exchange step. For instance, we synthesized and patterned $CsPbBr_{3-x}Cl_x$ NCs emitting at 447 nm, with $x \sim 1.5$ (Figure 3A,F). Alternatively, patterned $CsPbBr_3$ NCs can be transformed into $CsPbBr_{3-x}I_x$ NCs by treating the film with a solution of PbI_2/oleic acid/oleylamine in ethyl acetate (Figure 3C–D). Depending on the solution concentration and treatment time, various degrees of anion exchange occurred (Figure 3E). With this approach, $CsPbBr_3$ NCs emitting at 522 nm can be red-shifted to $CsPbBr_{3-x}I_x$ NCs emitting up to 653 nm, with $x \sim 2$ (Figure 3F). Although this anion-exchange process also improves the PLQY, a subsequent ligand exchange with trifluoracetic and butylamine can be included to further increase the PLQY. Chloride exchange was also attempted, but only a small (~10 nm) blue-shift was observed due to the low solubility of $PbCl_2$ in ethyl acetate (Figure S11).

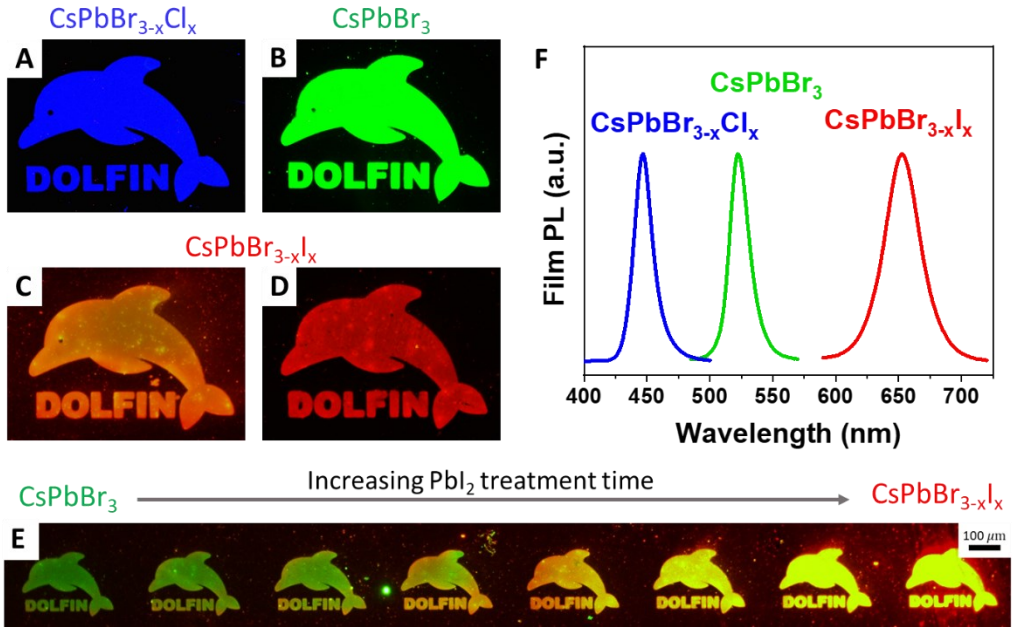

Figure 3. Fluorescence optical microscope images of micro-patterned films of $CsPbBr_{3-x}Cl_x$ (A), $CsPbBr_3$ (B) and $CsPbBr_{3-x}I_x$ (C&D). (E) Fluorescence image of a patterned $CsPbBr_3$ film that was slowly pulled out from a solution of PbI_2/oleic acid/oleylamine in ethyl acetate showing the progress of the anion exchange. (F) Film PL spectra of the $CsPbBr_{3-x}Cl_x$, $CsPbBr_3$, and $CsPbBr_{3-x}I_x$ NCs. The $CsPbBr_{3-x}I_x$ NCs were obtained by post-patterning anion exchange, while the $CsPbBr_{3-x}Cl_x$ NCs were synthesized directly.

We also explored the patterning of multiple layers of LHP NCs. Figure 4 shows patterning of a layer of $CsPbBr_{3-x}I_x$ NCs, followed by a second layer of $CsPbBr_3$ NCs. Anion exchange

between the two layers was prevented by an intermediate layer of poly(methyl methacrylate) (PMMA) before the deposition of the second layer. Deposition of the PMMA layer did not appear to affect the optical properties of the LHP NCs. Without this layer of PMMA, significant anion exchange was observed, resulting in changes of the PL emission wavelength (Figure S8).[53]

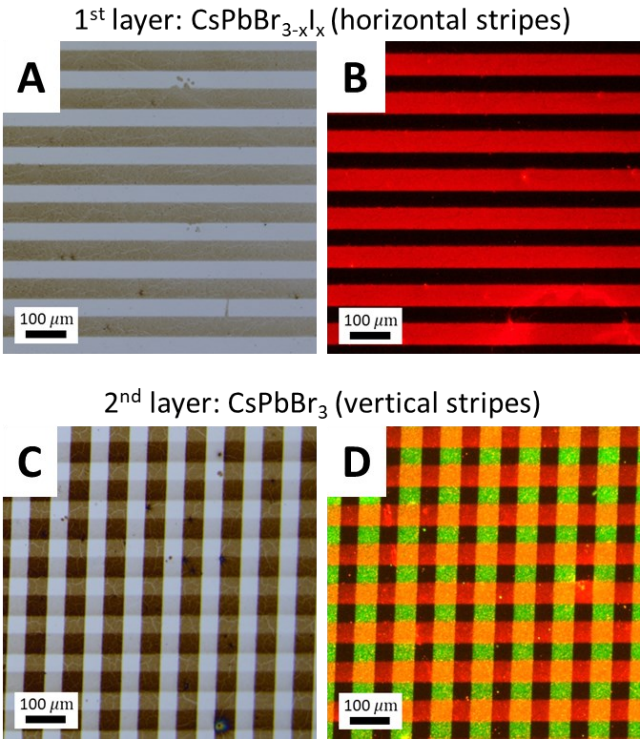

Figure 4. Bright-field (A & C) and fluorescence (B & D) optical microscope images after the patterning one or two layers of $CsPbX_3$ NC. A layer of PMMA was spin-coated on top of the red-emitting $CsPbBr_{3-x}I_3$ layer before the deposition and patterning of the second green-emitting $CsPbBr_3$ layer. The red channel in image (D) was boosted during image processing for ease of visibility.

An important advantage of this ligand-cleavage patterning approach over other polymer-based approaches is the short distance between the NCs which enables electronic communication and is important for applications such as LEDs, photodetectors, and other optoelectronic devices. As a proof of concept, we fabricated and tested simple photoconductor devices by depositing and patterning $CsPbBr_3$ NCs on top of an interdigitated gold electrode (Figure 5A–B). After treating the NCs with a trifluoracetic/butylamine solution, the devices exhibit a distinct photo-response to

violet light (Figure 5C), demonstrating the capability for charge injection or extraction into our NC layers. Although the performance of the photodetector shown here is lower than prior reports of optimized $CsPbBr_3$ films,[55-56] we believe that it can be improved with further optimization of the film thickness, NC packing density and ligand chemistry. In the future, more sophisticated ligand exchanges and surface treatments can be explored for the fabrication of high-efficiency patterned LED.[5-6]

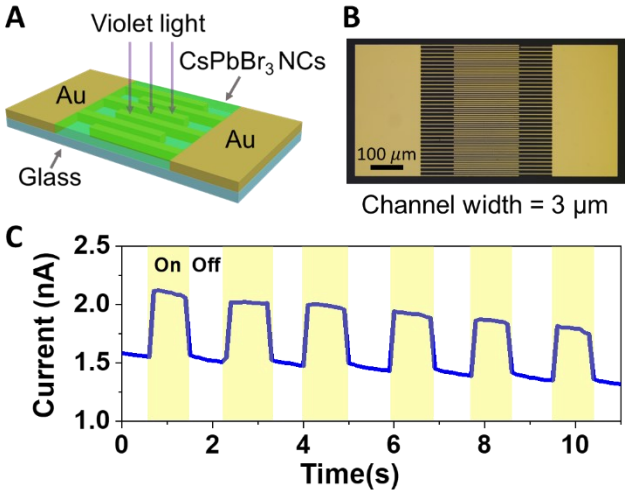

Figure 5. Photoconductivity of patterned $CsPbBr_3$ NCs after treatment with trifluoroacetic acid/butylamine. (A) Schematic of the device structure and testing condition. (B) Optical microscope image of the gold electrodes used. (C) Photocurrent–time response in the dark and under illumination with violet light (395 nm) with an applied voltage of 20 V.

In summary, we have demonstrated the patterning of $CsPbX_3$ NCs via the photoinduced cleavage of a bound oxime sulfonate ester (PA-480). The photosensitive PA-480 binds to the NC surface and cleaves at the N–O bond upon irradiation with 405 nm light, resulting in a change in the NC solubility in toluene allowing for pattern development. The patterned LHP NCs can be further treated to exchange the sulfonate ligands with more suitable ones such as trifluoroacetate, which allows for the improvement in the film PLQY up to 76%. The emission wavelength of the patterns can also be tuned across the visible by an on-film anion exchange or by using pre-synthesized alloyed NCs. Further, multilayer patterning of NC layers with different colors was also demonstrated. Finally, we fabricated simple photoconductive devices to show that patterned NC layers are amenable to electrical contact, which is an important prerequisite for various

optoelectronic applications. This approach shows the capability of carefully designed photosensitive ligands for patterning fragile nanomaterials such as the LHP NCs.

Methods

Synthesis of $CsPbX_3$ NCs. $CsPbBr_3$ NCs were synthesized by a modified benzoyl halide hot injection method.[38] Briefly cesium carbonate (16 mg, 0.049 mmol), lead acetate trihydrate (76 mg, 0.20 mmol), oleic acid (0.3 mL, 0.95 mmol), oleylamine (1 mL, 3.0 mmol) and octadecene (10 mL) were loaded into a 25 mL 3-neck round-bottom flask and dried under vacuum for 1 h at 115 °C. Subsequently, the temperature was increased to 170 °C under N_2 and benzoyl bromide (50 µL, 0.46 mmol) dissolved in 0.5 mL octadecene was swiftly injected. The reaction mixture was immediately cooled down with an ice-water bath. To purify the NCs, 1 mL of toluene was added to the crude solution followed by 40 mL of ethyl acetate. The resulting mixture was centrifuged (7 krpm, 6574 g-force) for 10 min with the temperature set at 0 °C. The supernatant was discarded, and the precipitate was brought into a N_2 glovebox and redispersed in 3 mL of toluene at a concentration of about 2.5 wt%. The solution was then centrifuged (4 krpm, 2213 g-force) for 1 min at room temperature to remove any insoluble contaminants. This stock NC solution was stored in the glovebox and used within 1-2 weeks. To synthesize $CsPbBr_{3-x}Cl_x$ NCs, a similar procedure was used except that a mixture of benzoyl bromide (25 µL) and benzoyl chloride (25 µL) dissolved in 0.5 mL of octadecene was used as the injection solution.

Patterning of LHP NCs. In air, 500 µL of ethyl acetate was added to 200 µL of the LHP NC stock solution to induce flocculation of NCs. The suspension was centrifuged (13.4 krpm, 12100 g) for 1 min. The supernatant was discarded, and the precipitate redissolved in 80 µL of chlorobenzene (or toluene). To this solution, 16 µL of PA-480 pre-dissolved in chlorobenzene (or toluene) at a concentration of 5 wt/vol% was added, resulting in a solution with about 5 wt% NC and 0.8 wt% PA-480. This solution was spincoated on either a silicon substrate or a glass cover slip. The substrate was then bound between a glass slide and a patterned chrome on quartz mask using two binder clips. This stack was then exposed to 405 nm light (M405LP1-C1, Thorlabs, measured power density ~30 mW/cm^2) for 10 – 30 s. After exposure, the substrate was immersed into a toluene developer for ~10 s and dried with a N_2 gun. Occasionally, a pre-exposure and a post-exposure baking step at 70 °C was used to increase the contrast. For multiple layer patterning,

an intermediate layer of PMMA (MW~120k, 2 wt/vol% in anisole) was spin-coated between each NC layer.

Ligand and anion exchange. To prepare the $PbBr_2$/OctAc/BuAm treatment solution, $PbBr_2$ (0.5 mmol, 183 mg) was dissolved in butylamine (3 mmol, 296 uL), octanoic acid (3 mmol, 475 uL) and hexane (300 uL) by stirring overnight at 70 °C (total volume ~ 1 mL). About 10 vol% of this solution (100 uL) was then mixed with 9.9 mL of ethyl acetate to give a solution with <5 mM $PbBr_2$ (saturated), 30 mM OctAc, 30 mM BuAm and 23 mM hexane. (White $PbBr_2$ slowly precipitates out, which indicates saturation.) To prepare the $PbBr_2$/OctAc/BuAm/TFA treatment solution, the same procedure was used but with trifluoroacetic acid (0.5 mmol, 38 uL) added to the starting solution which result in treatment solution of 5 mM TFA, <5 mM $PbBr_2$ (saturated), 30 mM OctAc, 30 mM BuAm and 23 mM hexane in ethyl acetate.

To carry out ligand exchange, the substrate with the patterned LHP NC layer was placed in a spin-coater and a ligand treatment solution was pipetted on the substrate and allowed to sit for ~10 s before spinning. This spin-coating step was then repeated another time. To carry out I^- anion exchange, the patterned substrates were immersed in a solution of PbI_2/oleic acid/oleylamine in ethyl acetate. The extend of the exchange depends on the PbI_2 concentration and the duration of treatment. After the appropriate amount of treatment time, the substrates were removed and blown dry with N_2. Subsequent treatment of the iodide-exchanged film with an ethyl acetate solution of 5 mM trifluoroacetate and 5 mM butylamine can be used to further improve the PLQY. These ligand/anion steps can be carried out in air when the humidity is low (*e.g.* in the winter months), but should be carried out in a glovebox when the humidity is high.

Photoconductivity measurement. The device electrodes (channel width = 3 μm, total channel length = 13.2 mm) were fabricated on glass *via* a standard photolithography process with a direct laser writer (Heidelberg MLA 150). The electrodes were deposited by electron-beam evaporation of a 5-nm Ti adhesion layer and a 100-nm Au layer (AJA ATC-Orion 8E). $CsPbBr_3$ NCs were deposited and patterned on the electrodes followed by a ligand exchange with trifluoroacetic/butylamine/$PbBr_2$. Electrical measurements were carried out in a N_2 glovebox with probes connected to a parameter analyzer (Agilent B1500A). Violet light illumination was provided by a violet LED flashlight (TaoTronics, wavelength = 395 nm).

Associated Content

Supporting Information. The supporting information is available free of charge at http://pubs.acs.org.

Chemicals, characterization techniques, film absorption spectra of LHP NCs with PA-480, absorption spectra of PA-480 upon irradiation, decomposition pathway of PA-480, fitting of XRD peaks using a multilayer diffraction model, TEM images of $CsPbBr_3$ NCs at each point of the patterning process, FTIR spectra of PA-480 before and after irradiation, LHP NC patterns with ILP-110N, optical microscope images of multilayer NCs without any intermediate layer, PLQY measurements in solution, PL lifetime measurements of films, PL shift after on-film chloride exchange

Author information

Corresponding author

* E-mail: dvtalapin@uchicago.edu

Notes

The authors declare no competing financial interests.

Acknowledgements

We would like to thank Dr. Xinzheng Lan for fabricating the electrodes for photoconductivity measurements. We also thank Dr. Himchan Cho and Dr. Igor Coropceanu for assistance with the absolute quantum yield measurements. The work on nanocrystal synthesis, surface functionalization and optical patterning was supported by NSF under award number CHE-1905290. The study of photochemistry of lead halide perovskite nanocrystals with photosensitive surface ligands was supported by the Department of Defense (DOD) Air Force Office of Scientific Research under grant number FA9550-18-1-0099. This work was also partially supported by the University of Chicago Materials Research Science and Engineering Center, which is funded by the National Science Foundation under award number DMR-2011854. Use of the Center for Nanoscale Materials, an Office of Science User Facilities operated for the U.S. Department of

Energy (DOE) Office of Science by Argonne National Laboratory, was supported by the U.S. DOE under Contract No. DE-AC02-06CH11357. This work made use of the Pritzker Nanofabrication Facility, which receives partial support from the SHyNE Resource, a node of the National Science Foundation's National Nanotechnology Coordinated Infrastructure (NSF ECCS-2025633).

References

1. Protesescu, L.; Yakunin, S.; Bodnarchuk, M. I.; Krieg, F.; Caputo, R.; Hendon, C. H.; Yang, R. X.; Walsh, A.; Kovalenko, M. V., Nanocrystals of Cesium Lead Halide Perovskites (CsPbX3, X = Cl, Br, and I): Novel Optoelectronic Materials Showing Bright Emission with Wide Color Gamut. *Nano Lett.* **2015,** *15* (6), 3692-3696.
2. Kovalenko, M. V.; Protesescu, L.; Bodnarchuk, M. I., Properties and potential optoelectronic applications of lead halide perovskite nanocrystals. *Science* **2017,** *358* (6364), 745-750.
3. Shamsi, J.; Urban, A. S.; Imran, M.; De Trizio, L.; Manna, L., Metal Halide Perovskite Nanocrystals: Synthesis, Post-Synthesis Modifications, and Their Optical Properties. *Chem. Rev.* **2019,** *119* (5), 3296-3348.
4. Nature MaterialsAkkerman, Q. A.; Rainò, G.; Kovalenko, M. V.; Manna, L., Genesis, challenges and opportunities for colloidal lead halide perovskite nanocrystals. *Nat. Mater.* **2018,** *17* (5), 394-405.
5. Kim, Y.-H.; Kim, S.; Kakekhani, A.; Park, J.; Park, J.; Lee, Y.-H.; Xu, H.; Nagane, S.; Wexler, R. B.; Kim, D.-H.; Jo, S. H.; Martínez-Sarti, L.; Tan, P.; Sadhanala, A.; Park, G.-S.; Kim, Y.-W.; Hu, B.; Bolink, H. J.; Yoo, S.; Friend, R. H.; Rappe, A. M.; Lee, T.-W., Comprehensive defect suppression in perovskite nanocrystals for high-efficiency light-emitting diodes. *Nat. Photonics* **2021,** *15* (2), 148-155.
6. Hassan, Y.; Park, J. H.; Crawford, M. L.; Sadhanala, A.; Lee, J.; Sadighian, J. C.; Mosconi, E.; Shivanna, R.; Radicchi, E.; Jeong, M.; Yang, C.; Choi, H.; Park, S. H.; Song, M. H.; De Angelis, F.; Wong, C. Y.; Friend, R. H.; Lee, B. R.; Snaith, H. J., Ligand-engineered bandgap stability in mixed-halide perovskite LEDs. *Nature* **2021,** *591* (7848), 72-77.
7. Zheng, X.; Yuan, S.; Liu, J.; Yin, J.; Yuan, F.; Shen, W.-S.; Yao, K.; Wei, M.; Zhou, C.; Song, K.; Zhang, B.-B.; Lin, Y.; Hedhili, M. N.; Wehbe, N.; Han, Y.; Sun, H.-T.; Lu, Z.-H.; Anthopoulos, T. D.; Mohammed, O. F.; Sargent, E. H.; Liao, L.-S.; Bakr, O. M., Chlorine Vacancy Passivation in Mixed Halide Perovskite Quantum Dots by Organic Pseudohalides Enables Efficient Rec. 2020 Blue Light-Emitting Diodes. *ACS Energy Lett.* **2020,** *5* (3), 793-798.
8. Jeon, S.; Lee, S. Y.; Kim, S.-K.; Kim, W.; Park, T.; Bang, J.; Ahn, J.; Woo, H. K.; Chae, J.-Y.; Paik, T.; Seong, T.-Y.; Oh, S. J., All-Solution Processed Multicolor Patterning Technique of Perovskite Nanocrystal for Color Pixel Array and Flexible Optoelectronic Devices. *Adv. Opt. Mater.* **2020,** *8* (17), 2000501.
9. Xing, D.; Lin, C.-C.; Ho, Y.-L.; Kamal, A. S. A.; Wang, I. T.; Chen, C.-C.; Wen, C.-Y.; Chen, C.-W.; Delaunay, J.-J., Self-Healing Lithographic Patterning of Perovskite Nanocrystals for Large-Area Single-Mode Laser Array. *Adv. Funct. Mater.* **2021,** *31* (1), 2006283.
10. Wang, Y.; Li, X.; Song, J.; Xiao, L.; Zeng, H.; Sun, H., All-Inorganic Colloidal Perovskite Quantum Dots: A New Class of Lasing Materials with Favorable Characteristics. *Adv. Mater.* **2015,** *27* (44), 7101-7108.
11. Yakunin, S.; Protesescu, L.; Krieg, F.; Bodnarchuk, M. I.; Nedelcu, G.; Humer, M.; De Luca, G.; Fiebig, M.; Heiss, W.; Kovalenko, M. V., Low-threshold amplified spontaneous emission and lasing from colloidal nanocrystals of caesium lead halide perovskites. *Nat. Commun.* **2015,** *6* (1), 8056.
12. Liu, C.; Zeng, Q.; Wei, H.; Yu, Y.; Zhao, Y.; Feng, T.; Yang, B., Metal Halide Perovskite Nanocrystal Solar Cells: Progress and Challenges. *Small Methods* **2020,** *4* (10), 2000419.

13. Swarnkar, A.; Marshall, A. R.; Sanehira, E. M.; Chernomordik, B. D.; Moore, D. T.; Christians, J. A.; Chakrabarti, T.; Luther, J. M., Quantum dot-induced phase stabilization of alpha-CsPbI3 perovskite for high-efficiency photovoltaics. *Science* **2016,** *354* (6308), 92-95.
14. Ramasamy, P.; Lim, D.-H.; Kim, B.; Lee, S.-H.; Lee, M.-S.; Lee, J.-S., All-inorganic cesium lead halide perovskite nanocrystals for photodetector applications. *Chem. Commun.* **2016,** *52* (10), 2067-2070.
15. Gandini, M.; Villa, I.; Beretta, M.; Gotti, C.; Imran, M.; Carulli, F.; Fantuzzi, E.; Sassi, M.; Zaffalon, M.; Brofferio, C.; Manna, L.; Beverina, L.; Vedda, A.; Fasoli, M.; Gironi, L.; Brovelli, S., Efficient, fast and reabsorption-free perovskite nanocrystal-based sensitized plastic scintillators. *Nat. Nanotechnol.* **2020,** *15* (6), 462-468.
16. Chen, Q.; Wu, J.; Ou, X.; Huang, B.; Almutlaq, J.; Zhumekenov, A. A.; Guan, X.; Han, S.; Liang, L.; Yi, Z.; Li, J.; Xie, X.; Wang, Y.; Li, Y.; Fan, D.; Teh, D. B. L.; All, A. H.; Mohammed, O. F.; Bakr, O. M.; Wu, T.; Bettinelli, M.; Yang, H.; Huang, W.; Liu, X., All-inorganic perovskite nanocrystal scintillators. *Nature* **2018,** *561* (7721), 88-93.
17. Utzat, H.; Sun, W.; Kaplan, A. E. K.; Krieg, F.; Ginterseder, M.; Spokoyny, B.; Klein, N. D.; Shulenberger, K. E.; Perkinson, C. F.; Kovalenko, M. V.; Bawendi, M. G., Coherent single-photon emission from colloidal lead halide perovskite quantum dots. *Science* **2019,** *363* (6431), 1068.
18. Wu, S.; Fan, Z.; Wang, W.; Fan, H.; Mei, Z.; Sun, D.; Cheng, X.; Zhao, X.; Tian, Y., Microfabricable ratiometric gaseous oxygen sensors based on inorganic perovskite nanocrystals and PtTFPP. *Sens. Actuators, B* **2018,** *271*, 104-109.
19. Park, S.; Cho, J.; Jeong, D.; Jo, J.; Nam, M.; Rhee, H.; Han, J. S.; Cho, Y. J.; Ju, B.-K.; Ko, D.-H.; Jang, H. S., Simultaneous enhancement of luminescence and stability of CsPbBr3 perovskite nanocrystals via formation of perhydropolysilazane-derived nanopatterned film. *Chem. Eng. J.* **2020,** *393*, 124767.
20. Liu, Y.; Li, F.; Qiu, L.; Yang, K.; Li, Q.; Zheng, X.; Hu, H.; Guo, T.; Wu, C.; Kim, T. W., Fluorescent Microarrays of in Situ Crystallized Perovskite Nanocomposites Fabricated for Patterned Applications by Using Inkjet Printing. *ACS Nano* **2019,** *13* (2), 2042-2049.
21. Altintas, Y.; Torun, I.; Yazici, A. F.; Beskazak, E.; Erdem, T.; Serdar Onses, M.; Mutlugun, E., Multiplexed patterning of cesium lead halide perovskite nanocrystals by additive jet printing for efficient white light generation. *Chem. Eng. J.* **2020,** *380*, 122493.
22. Palazon, F.; Akkerman, Q. A.; Prato, M.; Manna, L., X-ray Lithography on Perovskite Nanocrystals Films: From Patterning with Anion-Exchange Reactions to Enhanced Stability in Air and Water. *ACS Nano* **2016,** *10* (1), 1224-1230.
23. Dou, L.; Lai, M.; Kley, C. S.; Yang, Y.; Bischak, C. G.; Zhang, D.; Eaton, S. W.; Ginsberg, N. S.; Yang, P., Spatially resolved multicolor CsPbX3 nanowire heterojunctions via anion exchange. *Proc. Natl. Acad. Sci. U. S. A.* **2017,** *114* (28), 7216-7221.
24. Lin, C. H.; Zeng, Q.; Lafalce, E.; Yu, S.; Smith, M. J.; Yoon, Y. J.; Chang, Y.; Jiang, Y.; Lin, Z.; Vardeny, Z. V.; Tsukruk, V. V., Large-Area Lasing and Multicolor Perovskite Quantum Dot Patterns. *Adv. Opt. Mater.* **2018,** *6* (16), 1800474.
25. Ko, J.; Ma, K.; Joung, J. F.; Park, S.; Bang, J., Ligand-Assisted Direct Photolithography of Perovskite Nanocrystals Encapsulated with Multifunctional Polymer Ligands for Stable, Full-Colored, High-Resolution Displays. *Nano Lett.* **2021,** *21* (5), 2288-2295.
26. Ko, J.; Chang, J. H.; Jeong, B. G.; Kim, H. J.; Joung, J. F.; Park, S.; Choi, D. H.; Bae, W. K.; Bang, J., Direct Photolithographic Patterning of Colloidal Quantum Dots Enabled by UV-Crosslinkable and Hole-Transporting Polymer Ligands. *ACS Appl. Mater. Interfaces* **2020,** *12* (37), 42153-42160.
27. Kim, H.; Hight-Huf, N.; Kang, J.-H.; Bisnoff, P.; Sundararajan, S.; Thompson, T.; Barnes, M.; Hayward, R. C.; Emrick, T., Polymer Zwitterions for Stabilization of CsPbBr3 Perovskite Nanoparticles and Nanocomposite Films. *Angew. Chem. Int. Ed.* **2020,** *59* (27), 10802-10806.
28. Lee, H.; Jeong, J. W.; So, M. G.; Jung, G. Y.; Lee, C. L., Design of Chemically Stable Organic Perovskite Quantum Dots for Micropatterned Light-Emitting Diodes through Kinetic Control of a Cross-Linkable Ligand System. *Adv. Mater.* **2021**, e2007855.

29. Minh, D. N.; Eom, S.; Nguyen, L. A. T.; Kim, J.; Sim, J. H.; Seo, C.; Nam, J.; Lee, S.; Suk, S.; Kim, J., Perovskite Nanoparticle Composite Films by Size Exclusion Lithography. *Adv. Mater.* **2018,** *30* (39), 1802555.
30. Huang, X.; Guo, Q.; Yang, D.; Xiao, X.; Liu, X.; Xia, Z.; Fan, F.; Qiu, J.; Dong, G., Reversible 3D laser printing of perovskite quantum dots inside a transparent medium. *Nat. Photonics* **2019,** *14* (2), 82-88.
31. Zhan, W.; Meng, L.; Shao, C.; Wu, X.-g.; Shi, K.; Zhong, H., In Situ Patterning Perovskite Quantum Dots by Direct Laser Writing Fabrication. *ACS Photonics* **2021,** *8* (3), 765-770.
32. Rainò, G.; Becker, M. A.; Bodnarchuk, M. I.; Mahrt, R. F.; Kovalenko, M. V.; Stöferle, T., Superfluorescence from lead halide perovskite quantum dot superlattices. *Nature* **2018,** *563* (7733), 671-675.
33. Krieg, F.; Sercel, P. C.; Burian, M.; Andrusiv, H.; Bodnarchuk, M. I.; Stöferle, T.; Mahrt, R. F.; Naumenko, D.; Amenitsch, H.; Rainò, G.; Kovalenko, M. V., Monodisperse Long-Chain Sulfobetaine-Capped CsPbBr3 Nanocrystals and Their Superfluorescent Assemblies. *ACS Cent. Sci.* **2021,** *7* (1), 135-144.
34. Wang, Y.; Pan, J.-A.; Wu, H.; Talapin, D. V., Direct Wavelength-Selective Optical and Electron-Beam Lithography of Functional Inorganic Nanomaterials. *ACS Nano* **2019,** *13* (12), 13917-13931.
35. Wang, Y.; Fedin, I.; Zhang, H.; Talapin, D. V., Direct optical lithography of functional inorganic nanomaterials. *Science* **2017,** *357* (6349), 385-388.
36. Pan, J.-A.; Rong, Z.; Wang, Y.; Cho, H.; Coropceanu, I.; Wu, H.; Talapin, D. V., Direct Optical Lithography of Colloidal Metal Oxide Nanomaterials for Diffractive Optical Elements with 2π Phase Control. *J. Am. Chem. Soc.* **2021,** *143* (5), 2372-2383.
37. Cho, H.; Pan, J. A.; Wu, H.; Lan, X.; Coropceanu, I.; Wang, Y.; Cho, W.; Hill, E. A.; Anderson, J. S.; Talapin, D. V., Direct Optical Patterning of Quantum Dot Light-Emitting Diodes via In Situ Ligand Exchange. *Adv. Mater.* **2020,** *32* (46), 2003805.
38. Imran, M.; Caligiuri, V.; Wang, M.; Goldoni, L.; Prato, M.; Krahne, R.; De Trizio, L.; Manna, L., Benzoyl Halides as Alternative Precursors for the Colloidal Synthesis of Lead-Based Halide Perovskite Nanocrystals. *J. Am. Chem. Soc.* **2018,** *140* (7), 2656-2664.
39. Nenon, D. P.; Pressler, K.; Kang, J.; Koscher, B. A.; Olshansky, J. H.; Osowiecki, W. T.; Koc, M. A.; Wang, L.-W.; Alivisatos, A. P., Design Principles for Trap-Free CsPbX3 Nanocrystals: Enumerating and Eliminating Surface Halide Vacancies with Softer Lewis Bases. *J. Am. Chem. Soc.* **2018,** *140* (50), 17760-17772.
40. Di Stasio, F.; Christodoulou, S.; Huo, N.; Konstantatos, G., Near-Unity Photoluminescence Quantum Yield in CsPbBr3 Nanocrystal Solid-State Films via Postsynthesis Treatment with Lead Bromide. *Chem. Mater.* **2017,** *29* (18), 7663-7667.
41. Ahmed, T.; Seth, S.; Samanta, A., Boosting the Photoluminescence of CsPbX3 (X = Cl, Br, I) Perovskite Nanocrystals Covering a Wide Wavelength Range by Postsynthetic Treatment with Tetrafluoroborate Salts. *Chem. Mater.* **2018,** *30* (11), 3633-3637.
42. Imran, M.; Ijaz, P.; Goldoni, L.; Maggioni, D.; Petralanda, U.; Prato, M.; Almeida, G.; Infante, I.; Manna, L., Simultaneous Cationic and Anionic Ligand Exchange For Colloidally Stable CsPbBr3 Nanocrystals. *ACS Energy Lett.* **2019,** *4* (4), 819-824.
43. Krieg, F.; Ochsenbein, S. T.; Yakunin, S.; ten Brinck, S.; Aellen, P.; Süess, A.; Clerc, B.; Guggisberg, D.; Nazarenko, O.; Shynkarenko, Y.; Kumar, S.; Shih, C.-J.; Infante, I.; Kovalenko, M. V., Colloidal CsPbX3 (X = Cl, Br, I) Nanocrystals 2.0: Zwitterionic Capping Ligands for Improved Durability and Stability. *ACS Energy Lett.* **2018,** *3* (3), 641-646.
44. Koscher, B. A.; Swabeck, J. K.; Bronstein, N. D.; Alivisatos, A. P., Essentially Trap-Free CsPbBr3 Colloidal Nanocrystals by Postsynthetic Thiocyanate Surface Treatment. *J. Am. Chem. Soc.* **2017,** *139* (19), 6566-6569.
45. De Roo, J.; Ibáñez, M.; Geiregat, P.; Nedelcu, G.; Walravens, W.; Maes, J.; Martins, J. C.; Van Driessche, I.; Kovalenko, M. V.; Hens, Z., Highly dynamic ligand binding and light absorption coefficient of cesium lead bromide perovskite nanocrystals. *ACS nano* **2016,** *10* (2), 2071-2081.

46. Palm, A.; Werbin, H., The Infrared Spectra of Alpha and Beta Oximes. *Can. J. Chem.* **1953,** *31* (11), 1004-1008.
47. Goubeau, J.; Fromme, I., Beiträge zur Kenntnis der Stickstoff—Sauerstoff-Bindung. I. N-O-Bindungen ohne Mesomerie. *Zeitschrift für anorganische Chemie* **1949,** *258* (1-2), 18-26.
48. Perez De Berti, I. O.; Cagnoli, M. V.; Pecchi, G.; Alessandrini, J. L.; Stewart, S. J.; Bengoa, J. F.; Marchetti, S. G., Alternative low-cost approach to the synthesis of magnetic iron oxide nanoparticles by thermal decomposition of organic precursors. *Nanotechnology* **2013,** *24* (17), 175601.
49. Yang, D.; Li, X.; Zhou, W.; Zhang, S.; Meng, C.; Wu, Y.; Wang, Y.; Zeng, H., CsPbBr3 Quantum Dots 2.0: Benzenesulfonic Acid Equivalent Ligand Awakens Complete Purification. *Adv. Mater.* **2019,** *31* (30), 1900767.
50. Toso, S.; Baranov, D.; Altamura, D.; Scattarella, F.; Dahl, J.; Wang, X.; Marras, S.; Alivisatos, A. P.; Singer, A.; Giannini, C.; Manna, L., Multilayer Diffraction Reveals That Colloidal Superlattices Approach the Structural Perfection of Single Crystals. *ACS Nano* **2021,** *15* (4), 6243-6256.
51. Dahl, J. C.; Wang, X.; Huang, X.; Chan, E. M.; Alivisatos, A. P., Elucidating the Weakly Reversible Cs–Pb–Br Perovskite Nanocrystal Reaction Network with High-Throughput Maps and Transformations. *J. Am. Chem. Soc.* **2020,** *142* (27), 11915-11926.
52. Liu, Z.; Bekenstein, Y.; Ye, X.; Nguyen, S. C.; Swabeck, J.; Zhang, D.; Lee, S.-T.; Yang, P.; Ma, W.; Alivisatos, A. P., Ligand Mediated Transformation of Cesium Lead Bromide Perovskite Nanocrystals to Lead Depleted Cs4PbBr6 Nanocrystals. *J. Am. Chem. Soc.* **2017,** *139* (15), 5309-5312.
53. Akkerman, Q. A.; D'Innocenzo, V.; Accornero, S.; Scarpellini, A.; Petrozza, A.; Prato, M.; Manna, L., Tuning the Optical Properties of Cesium Lead Halide Perovskite Nanocrystals by Anion Exchange Reactions. *J. Am. Chem. Soc.* **2015,** *137* (32), 10276-10281.
54. Nedelcu, G.; Protesescu, L.; Yakunin, S.; Bodnarchuk, M. I.; Grotevent, M. J.; Kovalenko, M. V., Fast Anion-Exchange in Highly Luminescent Nanocrystals of Cesium Lead Halide Perovskites (CsPbX3, X = Cl, Br, I). *Nano Lett.* **2015,** *15* (8), 5635-5640.
55. Li, X.; Yu, D.; Cao, F.; Gu, Y.; Wei, Y.; Wu, Y.; Song, J.; Zeng, H., Healing All-Inorganic Perovskite Films via Recyclable Dissolution–Recyrstallization for Compact and Smooth Carrier Channels of Optoelectronic Devices with High Stability. *Adv. Funct. Mater.* **2016,** *26* (32), 5903-5912.
56. Dong, Y.; Gu, Y.; Zou, Y.; Song, J.; Xu, L.; Li, J.; Xue, J.; Li, X.; Zeng, H., Improving All-Inorganic Perovskite Photodetectors by Preferred Orientation and Plasmonic Effect. *Small* **2016,** *12* (40), 5622-5632.